Measurements of Electron Energy Distributions in an Ion Thruster

Y. Hayakawa,* K. Miyazaki,* and S. Kitamura†
National Aerospace Laboratory, Chofu, Tokyo, Japan

This paper describes electron energy distributions measured in the discharge chamber of a 14-cm ring-cusp xenon ion thruster. The electron energy distributions were acquired by processing Langmuir probe characteristics measured at more than twenty points in the discharge chamber. The results show that a narrow electron beam is emitted from the hollow cathode and flows along the center line of the discharge chamber. The energies of the beam electrons (or primary electrons) are far from mono-energetic and their density is higher than that of the thermalized or Maxwellian electrons near the hollow cathode. The electron beam abruptly spreads in the downstream region of the discharge chamber, however, a small fraction of these electrons have energies greater than that associated with the cathode-to-plasma potential difference and they are able to reach the screen grid which is held at cathode potential. Many ions, which appear to be produced in the electron beam, concentrate near the center line of the discharge chamber.

Nomenclature

e = electronic charge
$f(V)$ = electron energy distribution function
I_e = probe electron current
I_i = ith element of arrayed currents
I_i'' = second derivative of I_i
m_e = electron mass
N = odd number
N_e = number density of electrons
S = probe surface area
V = potential difference between probe and plasma potential
V_i = probe voltage corresponding to I_i
V_p = probe voltage
X_i = ith element of arrayed values
X_i' = a value corresponding to X_i after smoothing
ΔV = voltage difference between V_i and V_{i+1}

Introduction

ION thrusters show higher efficiencies than other electric thrusters. The efficiency of an electron-bombardment type ion thruster depends mainly on the performance of the thruster discharge chamber. The lower the electric power required in the discharge chamber to supply the ions required by the ion extraction system, the better. Ions are produced by electrons, which are emitted from the hollow cathode and collide with propellant atoms, however, only those electrons which have sufficient energy to excite or ionize the atoms are important. Consequently, an understanding of the physical distribution of those electrons in the chamber is an important precursor to improving discharge chamber performance.

In a prior effort, Langmuir probe-current contour maps were generated for the discharge chamber of a 12-cm-diameter ion thruster by physically sweeping a probe held at cathode potential through the discharge chamber which had a baffle plate in front of the hollow cathode.[1] Orginally, it was believed that the current to such a probe would be almost equal to the ion current on the basis that electrons would be unable to reach the probe. This belief was strengthened by the observation that current flowing to the screen grid, which is held at cathode potential, was always positive. This suggested the ion current was greater than the electron current. However, it was determined that the current to the screen grid turned negative when the discharge current was increased in another thruster which had no baffle. This suggests that electrons, which have more energy than they had after they were accelerated away from the cathode, exist in the discharge chamber. The flow, or leakage, of such very-high-energy electrons to the screen grid means that input electric power is being lost and, consequently, thruster efficiency is being degraded. The prevention of such electron flow will improve the discharge chamber, and a knowledge of the electron energy distribution may help to make such improvements.

If the electron energy distribution obeys Maxwell-Boltzmann's law, the information about the high-energy electrons would be given by electron temperature and total electron density data which are quite easily acquired by a Langmuir probe. In general, the distribution in the discharge chamber does not obey the law. Many papers have been published about the measurement of electron energy distribution,[2-6] but no measurements have been made in a discharge chamber of an ion thruster under operation. Such measurement has been made and the results will be shown here. The results can assist in designing future ion thruster discharge chambers.

Theory of Measurement

In the case of collision-free and field-free plasmas, the electron energy distribution is related to the second derivative of probe electron current with respect to probe voltage by[7]

$$f(V) = \frac{2}{eS}\left(\frac{2m_eV}{e}\right)^{1/2}\frac{d^2I_e}{dV_p^2} \tag{1}$$

The probe electron current can be replaced by total probe current because ion current is negligible. Electron density is given by integrating "$f(V)$" from $V = 0$ through $V = \infty$, that is

$$N_e = \int_0^\infty f(V)\,dV \tag{2}$$

Presented as Paper 89-2715 at the AIAA 25th Joint Propulsion Conference, Monterey, CA, July 10–12, 1989; received May 14, 1990; revision received Nov. 5, 1990; accepted for publication Nov. 19, 1990.

*Research Officer, Space Technology Research Group.
†Senior Research Officer, Space Technology Research Group. Member AIAA.

In the case of the plasma in the discharge chamber of a ring-cusp ion thruster, the pressure of the propellant is sufficiently low (lower than 1×10^{-1} Pa), so the effect of collisions in the probe sheath is negligible. The effect of magnetic flux density, on the other hand, may not be negligible. Equation (1) may not be strictly applicable in this case and the results may require correction. The accuracy of Eq. (1) was not evaluated in this study, but three kinds of Langmuir probes were used to estimate how the difference of probe geometry affects the results.

Apparatus and Procedure

A cross sectional view of the 14-cm-diameter ring-cusp ion thruster used in this study is shown in Fig. 1. Three samarium cobalt magnet rings are on the side wall and two on the upstream plate. Each magnet ring is composed of 12 magnets, so the side wall forms a dodecagonal tube. The thickness of the side wall is 1 mm and that of the upstream plate is 2 mm. Both the wall and plate are made of soft iron. The magnetic field produced is shown in Figs. 2 and 3. Figure 2 shows magnetic field lines and Fig. 3 shows magnetic flux density contours which are drawn at every 5 mT up to 200 mT (the magnetic field was calculated by a program which was derived from NONSAP "NONlinear Structural Analysis Program").

The small circles accompanied by numbers in Figs. 1, 2, and 3 show the Probe-Positions (PP) at which the measurements were made. Probe-Position 1 through 7 and 29 lie on the center line of the discharge chamber which is concentric with the hollow cathode. Probe-Position 1 through 7 are evenly spaced at 12 mm with PP 1 about 16 mm downstream of the hollow cathode and PP 29 lies 3 mm downstream of PP 7 and about 4 mm upstream of the cold screen grid. Probe-Position 8 through 14 and 30 lie on the line parallel to the centerline of the discharge chamber and each lies on the same axial position as PP 1 through 7 and 29 along the centerline. Probe-Position 1 and PP 8 are spaced by 20 deg (see Figs. 4 and 5). Probe-Position 15 through 21, 5, and 12 lie on an arc (see Figs. 4 and 5) close to the plane on which one of the magnet rings lies and are evenly spaced by 10 deg except PP 21. Similarly from PP 22 through 28, 3, and 10 lie on an arc close to the plane which lies evenly spaced from the two nearest magnet rings, and are evenly spaced by 10 degrees except PP 28. Both PP 21 and PP 28 depend on the shape of the probe and are spaced from the wall of the chamber by approximately 1 mm. Figure 4 shows the shapes of the Langmuir probes used in this experiment. The diameter of the Probe 1 wire seems large compared with that of the sphere, but it was impossible to make the same sphere with thinner wire. The shaft of the probe penetrates the upstream plate of the discharge chamber, and is connected to a probe driver. The probe driver can move the shaft of the probe axially and rotate it around its axis, so that the tip of the probe can reach nearly any r, z locations of the discharge chamber.

Figure 6 shows the electric circuit used for the measurement. A triangle wave is generated by the oscillator and amplified by the linear amplifier up to 72 V peak-to-peak. The frequency of the wave is about 50 Hz and is determined by the speed of the A/D converter. The bipolar power supply shifts the center of the wave 10 V positive of cathode potential so the amplitude of the 72 V wave will be sufficient to both stop very-high-energy electrons and reach plasma potential. The probe current is transformed to voltage by the 5 ohm resistor. The voltage drop by the resistor is negligible because the probe current is less than 2 mA. Both the probe current and the probe voltage are measured through the isolation

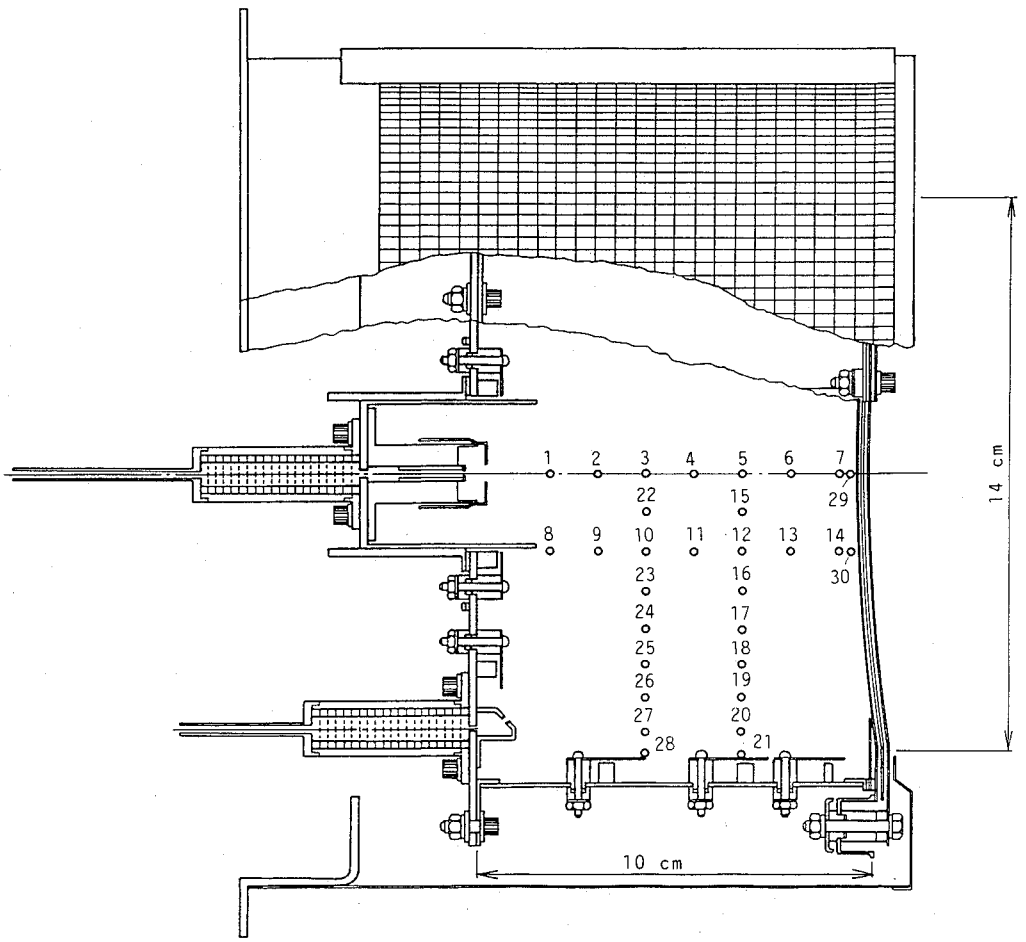

Fig. 1 Cross-sectional view of ring-cusp ion thruster.

amplifier because the discharge chamber is held at high voltage, more than 1000 V. A Low-Pass-Filter (LPF) is built into each isolation amplifier. To reduce noise, the signal of the current passes through the LPF while that of the voltage does not. One kHz was chosen as the Cut-Off-Frequency (COF) of the LPF because the noise removed with 10 kHz or 100 kHz COFs was insufficient to prevent noise induced signal distortion, and the original signal was badly deformed with 100 Hz COF. Both signals are alternately converted to digital values by the high-speed 12-bit A/D converter (200 kHz/ch) and successively transferred to the disktop computer. One set of values, 4096 pairs of the current and the voltage, is transferred to the computer during a positive slope of the triangle wave (about 10 ms long). It is difficult to get a smooth second-derivative curve from a single probe characteristic, so the measurements have to be repeated many times and the results have to be averaged. There is not enough memory on the computer to store every value, so each value has to be averaged. Voltage and current readings are added separately to their base registers during the two and a half cycles (about 50 ms long) right after they are acquired. Consequently, it takes about 60 ms to get a set of current-voltage pairs.

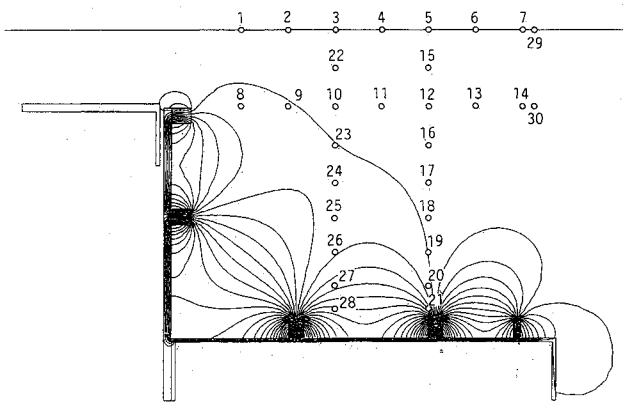

Fig. 2 Magnetic field lines (computer generated).

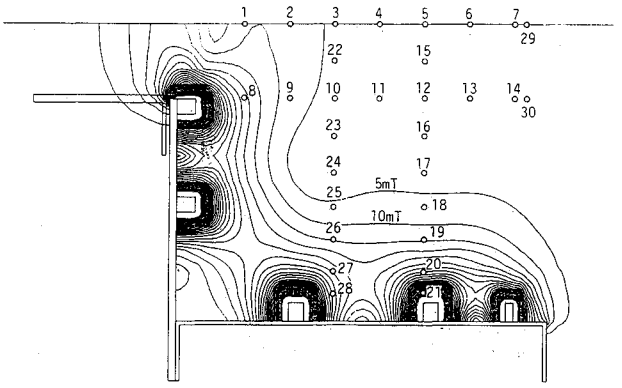

Fig. 3 Magnetic flux density contours (computer generated).

The number of measurements needed to generate a smooth second derivative was investigated and it was found that the second derivative was much smoother when 1024 averaged data pairs were collected than it was with either 256 or 512 data pairs. Increasing to 8192 data pairs gave no additional improvement. So 1024 was chosen as the number of the measurements in this study. Actually, 4096 discrete values, corresponding to 12 bits, of current and voltage are compressed to obtain the 1024 discrete current/voltage data pairs. This averaging procedure is used because 4096 data pairs cannot be displayed on the computer and because the influence of the A/D converter's idiosyncrasy must be reduced.

The second derivative of the averaged probe characteristics is given by

$$I_i'' = (I_{i+1} + I_{i-1} - 2I_i)/\Delta V^2 \tag{3}$$

In this study, "ΔV" is a constant and its value is 78.125 mV.

The second derivative curve is smoothed three times by applying the partial averaging method. One of the results is given by

$$X_i' = (X_{i-(N-1)/2} + X_{i-(N-3)/2} + \cdots + X_i + \cdots + X_{i+(N-3)/2} + X_{i+(N-1)/2})N \tag{4}$$

"X_i'" is not the ith element of the smoothed series of values because both the first and the last $(N-1)/2$ values do not exist. The number "N" should be chosen to limit deformation of the original curve. A value of 21 was applied to all curves in this study to assume consistency even though this number was generally larger than necessary. A Gaussian distribution

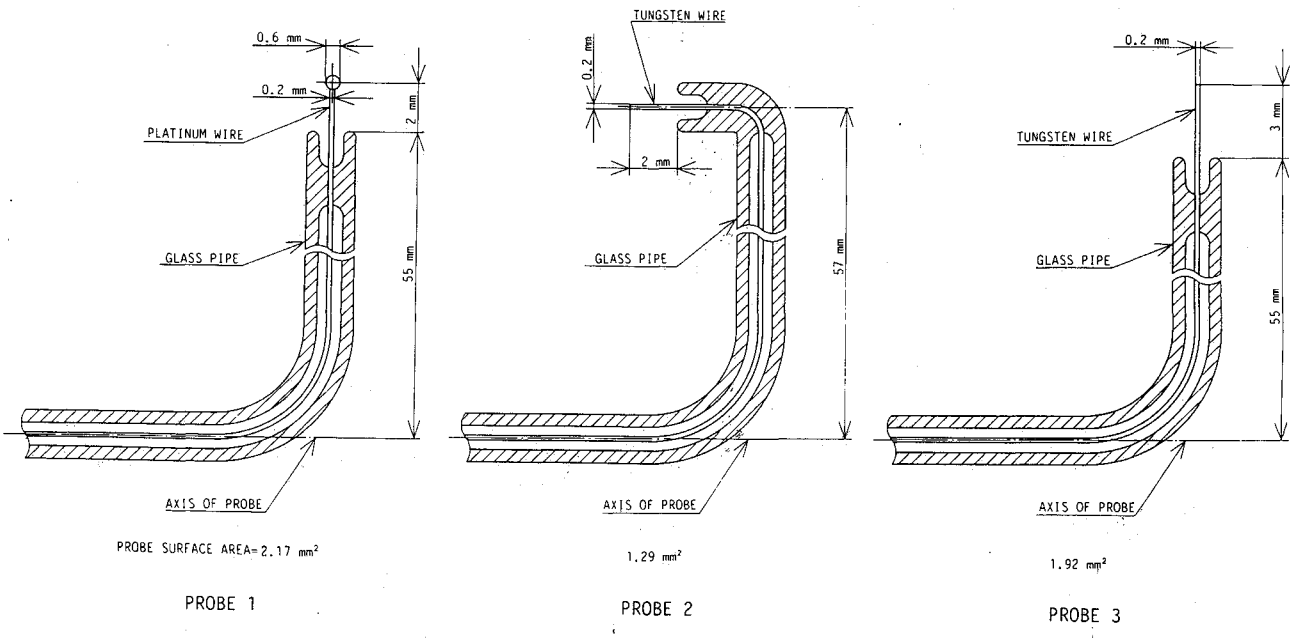

Fig. 4 Cross-sectional views of Langmuir probes.

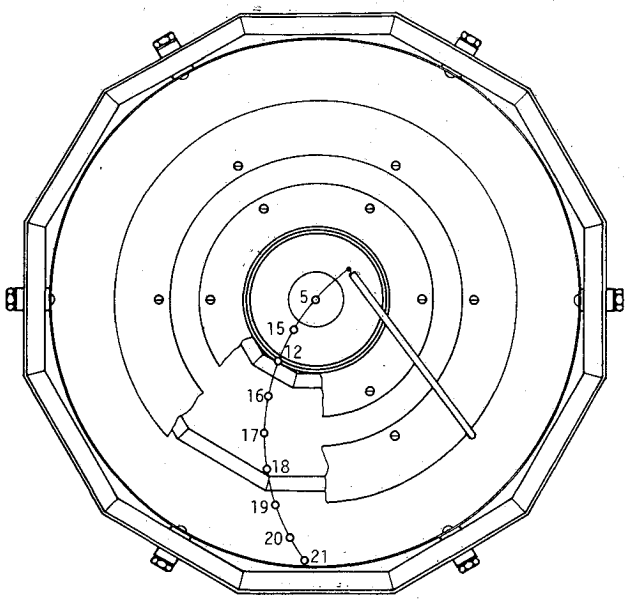

Fig. 5 Front view of discharge chamber.

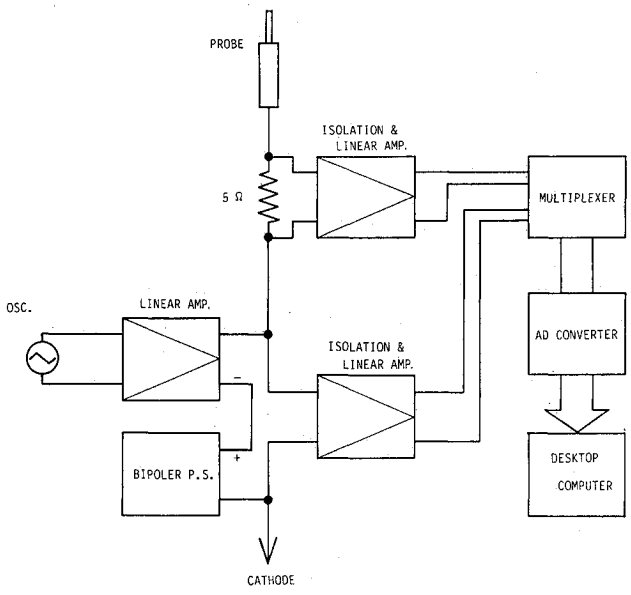

Fig. 6 Electric circuit.

with 2 eV full width at half maximum (FWHM) becomes a single peak distribution with 2.81 eV FWHM through a series of averaging. The peak height will be reduced to 77% of its original height. If there are mono-energetic primary electrons,[6] they will be easily identified.

The thruster was operated in our vacuum chamber[8] for all tests. Table 1 shows the fixed thruster operational parameters maintained during the tests by current-controlled or voltage-controlled power supplies and mass flow controllers. The propellant utilization efficiency was set near 90% before beginning the measurements by controlling discharge current. This current was then held constant by the current-controlled power supply while the measurements were being made.

The ion thruster operated more than 1 h before a series of measurements were made to avoid temperature changes that could otherwise occur during the 1½ h needed to collect the data. The triangle wave was applied to the probe right after the thruster was operating to clean the probe surface, and the measurements were initiated only after the reproducibility of test results had been assumed.

Table 1 Fixed thruster operational parameters

Screen grid potential	1000 V
Accelerator grid potential	−800 V
Cathode keeper current	0 A
Neutralizer keeper current	0.5 A
Propellant flowrate	
Cathode	53 mAeq
Main	478 mAeq
Neutralizer	40 mAeq

Table 2 Measured thruster operational parameters

Accelerator grid current	2.0–2.1 mA
Neutralizer keeper voltage	22.7–23.0 V

Table 3 Measured thruster operational parameters[a]

Probe position	Discharge voltage, V	Beam current, mA	Propellant utilization efficiency, %	Ion production cost, W/A
1	36.0	484	91.1	238
2	36.4	484	91.1	241
3	36.0	481	90.6	240
4	36.0	480	90.4	240
5	35.9	478	90.0	240
6	35.8	478	90.0	240
7	35.6	477	89.8	238
8	35.9	483	91.0	237
9	35.7	482	90.8	236
10	35.7	480	90.4	237
11	35.6	479	90.2	237
12	35.5	477	89.8	237
13	35.5	476	89.6	238
14	35.5	476	89.6	238
15	35.2	475	89.5	236
16	35.3	477	89.8	235
17	35.3	477	89.8	235
18	35.2	478	90.0	234
19	35.3	479	90.2	234
20	35.4	480	90.4	235
21	35.3	481	90.6	233
22	35.0	474	89.3	234
23	35.1	477	89.8	234
24	35.1	478	90.0	233
25	35.1	478	90.0	233
26	34.9	478	90.0	231
27	35.0	480	90.4	232
28	35.2	480	90.4	233
29	35.8	477	89.8	239
30	35.6	477	89.8	238
1	35.0	477	89.8	233

[a](Probe 1: Spherical); Discharge current = 3.19 A; Background pressure = 1.8×10^{-4} Pa.

Results

Tables 2, 3, 4, and 5 show the operating parameters measured while the time measurements were being made. In these tables, the propellant utilization efficiency does not include the flowrate through the neutralizer. For all data, the probe location was varied in sequence as follows: 1 through 7, and 29, then 8 through 14, and 30 followed by 21 through 15, and finally 28 through 22. After a series of measurements, the operational parameters were measured with the probe at PP 1 to document any change. The final values are shown at the bottom of the tables. The change of the discharge voltage were 1.0, 1.1, and 0.7 V for each of the three sets of data collected (Tables 3, 4 and 5). Although these parameters could be affected by probe position, its effect on the parameters was generally negligible.

Figure 7 shows a typical probe characteristic and its second derivative at PP 1 with Probe 1. Even with the second deriv-

Table 4 Measured thruster operational parameters[a]

Probe position	Discharge voltage, V	Beam current, mA	Propellant utilization efficiency, %	Ion production cost, W/A
1	37.3	484	91.1	245
2	36.7	480	90.4	244
3	36.6	478	90.0	244
4	36.5	477	89.8	244
5	36.4	475	89.5	244
6	36.3	477	89.8	243
7	36.4	478	90.0	243
8	36.3	483	91.0	240
9	36.3	481	90.6	241
10	36.2	479	90.2	240
11	36.2	478	90.2	241
12	36.1	475	89.5	242
13	36.0	476	89.6	241
14	36.1	477	89.8	241
15	36.0	476	89.6	241
16	36.1	477	89.8	241
17	36.2	479	90.2	240
18	36.1	478	90.0	240
19	36.1	478	90.0	240
20	36.0	478	90.0	239
21	36.2	480	90.4	240
22	35.8	477	89.8	239
23	35.9	480	90.4	238
24	36.1	482	90.8	238
25	36.0	482	90.8	238
26	36.0	484	91.1	237
27	36.0	484	91.1	237
28	36.0	485	91.3	236
1	36.6	483	91.0	241

[a](Probe 2: Cylindrical); Discharge current = 3.18 A; Background pressure = 1.8×10^{-4} Pa.

Table 5 Measured thruster operational parameters[a]

Probe position	Discharge voltage, V	Beam current, mA	Propellant utilization efficiency, %	Ion production cost, W/A
1	34.4	474	89.3	221
2	34.5	471	88.7	224
3	34.1	467	87.9	223
4	34.0	466	87.8	223
5	34.0	464	87.4	223
6	33.9	464	87.4	223
7	33.8	464	87.4	222
8	33.7	470	88.5	218
9	33.5	467	87.9	218
10	33.5	466	87.8	219
11	33.5	464	87.4	219
12	33.4	463	87.2	219
13	33.4	462	87.0	220
14	33.4	462	87.0	220
15	33.0	459	86.4	219
16	33.0	462	87.0	216
17	33.1	463	87.2	217
18	33.2	465	87.6	217
19	33.2	465	87.6	217
20	33.1	466	87.8	216
21	33.1	467	87.9	216
22	32.6	460	86.6	215
23	32.6	462	87.0	214
24	32.6	462	87.0	214
25	32.7	463	87.2	214
26	32.6	463	87.2	213
27	32.7	464	87.4	214
28	33.9	466	87.8	214
29	33.6	463	87.2	221
30	33.3	462	87.0	219
1	33.0	465	87.6	215

[a](Probe 3: Cylindrical); Discharge current = 3.4 A; Background pressure = 1.9×10^{-4} Pa.

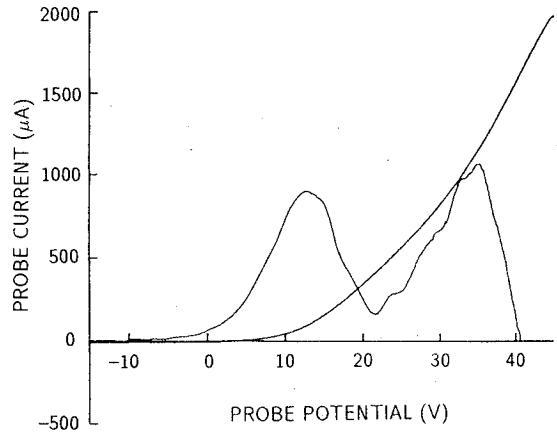

Fig. 7 Probe characteristic and second derivative at PP 1.

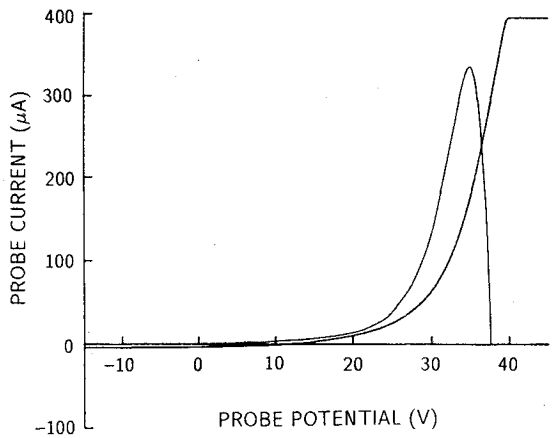

Fig. 8 Probe characteristic and second derivative at PP 18.

ative smoothed by the partial averaging method, there is still some unevenness that can be seen. Some of this unevenness is reproducible, but some is not. It was thought that irreproducible unevenness was caused by noises and might be reduced by increasing the number of probe characteristics being averaged. The fact that the unevenness was not reduced by increasing the number up to 8192 suggests that the plasma to be measured was not only fluctuating around an averaged condition, but also the averaged condition itself was changing. Consequently, to increase the number of the curves without reducing the period of the measurement was useless. In this region, the plasma was originally unsteady, that is, each probe characteristic, which was to be added up to give an averaged characteristic, differed significantly from others even though the approximate structure was almost the same. Consequently, many probe characteristics were needed to get a smooth averaged probe characteristic. In order to get smoother, more accurate probe characteristics, it would be necessary to increase the speed of data collection.

Figure 8 shows another typical probe characteristic and its second derivative at PP 18 with Probe 1. In this region, the plasma was steady and each measurement gives almost the same result as the next. As a result, the number of probe characteristics to be added to get a good averaged characteristic could be reduced.

Figure 9 shows electron energy distributions measured using Probe 1, and the corresponding data is given in Table 3. Each distribution is shown as a function of the voltage measured with respect to cathode potential. Plasma potential is given as the contact point between the right-end of the curve and the baseline. Some distribution curves acquired on the center line have two peaks while others have only one. The

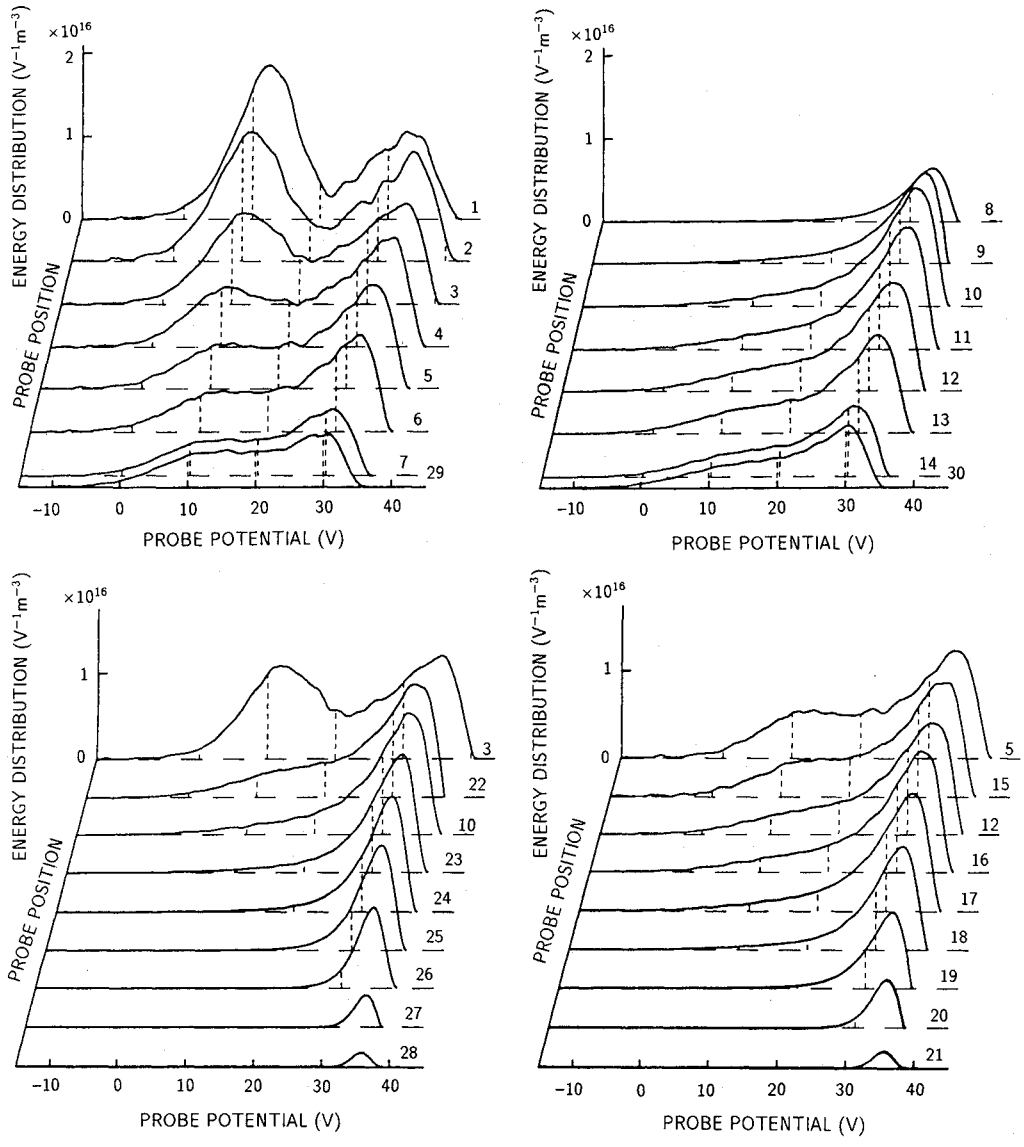

Fig. 9 Electron energy distribution with Probe 1 for Table 3 conditions.

right peaks of the two-peak distributions or the peaks of the one-peak distributions show groups of low energy electrons. These peaks are composed of both the electrons which lose their original energy through collisions and the electrons released as a consequence of ionization. The resulting peaks are suggestive of a Maxwellian distribution. The heights of these peaks are approximately constant in the region where magnetic flux density is lower than 10 mT. The left peak of two-peak distributions show groups of primary electrons which have not had sufficient inelastic collisions to lose much energy. They have some spread in their energy and the left-hand tails of the peaks extend to value negative of cathode potential. This suggests that some electrons have more energy than they could obtain as a result of being accelerated away from the cathode. The peaks of these bumps decrease as the probe is moved downstream and they eventually disappear. The fact that no such bump can be seen except on the center line (PP 1 through 7) suggests that the primary electrons are highly directional. Such electrons might be called "beam electrons." The potential difference between cathode potential and the left peak is about 12 V and the ionization potential of xenon is 12.1 V. This suggests that the primary electrons are composed mainly of the electrons which were emitted directly from the cathode, those that have had one inelastic ionizing collision, and those which were produced by the ionization event. The reason why the primary electrons are far from mono-energetic may be related to the fact that they have many collisions before they pass through the orifice of the hollow cathode.

Influence of Probe Shape and Area

Figure 10 shows electron energy distributions measured with Probe 2 and the corresponding data in Table 4. At PP 1, these data exhibit a peak near a 30-V probe potential (Maxwellian peak) which is similar in magnitude to the one in Fig. 9. The peak near 10 V (beam electron peak) is considerably higher in Fig. 10 than in Fig. 9. The opposite case of this can be expected because the beam electrons are nonisotropic while the Maxwellian electrons are isotropic. The total probe surface areas, which are used to compute the energy distributions yields proper values for the isotropic Maxwellian electrons. The distribution associated with the beam electrons are, however, in error for Figs. 9 and 10 because the probe cross-sectional area (normal to the beam) is the appropriate area in these cases. This area would be greater for Probe 1 than that for Probe 2 so the beam electron peak in Fig. 9 is expected to be higher than that in Fig. 10. Actually this expectation is realized at PPs 6 and 7. The reason why the expectation is not realized at PP 1 might be explained as follows: The beam electrons do not flow exactly on the centerline of the discharge

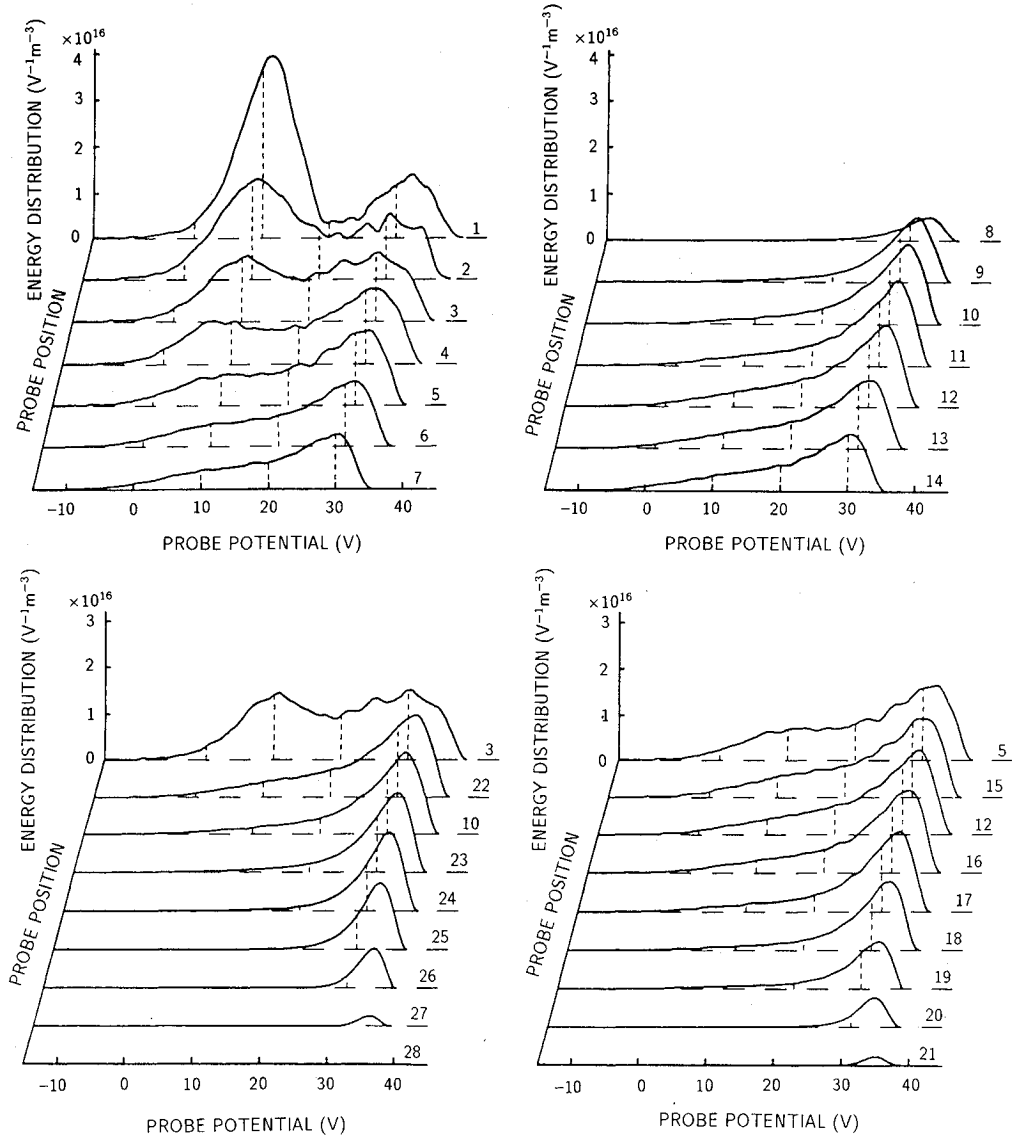

Fig. 10 Electron energy distribution with Probe 2 for Table 4 conditions.

chamber for some reason or other (see Fig. 11). It is rated that the tip of the probe in PP 1 was closer to the center of the electron beam for Probe 2 than that for Probe 1.

The electron energy distributions measured with Probe 3 were very similar to those shown in Fig. 9 except for the peak heights of the primary electrons. The diameter of the sphere of Probe 1 was not large enough compared to that of the wire, so the probe might not behave as a spherical probe in which the influence of the wire could be neglected.

It can be affirmed that three kinds of probes showed very similar pictures concerning Maxwellian electrons. Minute differences about Maxwellian electrons appear to be based on both inconsistent discharge conditions and the effects of the probe supports. On the other hand, the measurement of the primary electrons is considerably affected by the probe shape. This is unavoidable because the primary electrons are highly directional. In general, the probe cross-sectional area which is normal to the primary electron flow should represent the probe area in order to discuss the primary electrons quantitatively.

On this particular experiment, the probe position with respect to the electron beam appears to have the greatest influence to quantify the primary electrons. The electron beam is not guaranteed to flow just on the center line of the discharge chamber although that is where it is most expected. A more sophisticated system to move a probe to any position will be required to seek a finer picture of the primary electrons.

Spatial Distribution of High Energy Electrons and Ions

As has been mentioned before, high-energy and highly directional electrons were flowing along the center line. The relative intensity of the electron beam can be easily found provided an exact energy distribution is not required. The needed data are obtained by sweeping a probe through the discharge chamber twice: once at a potential negative enough to repel all electrons and once again at a potential selected to repel only low energy electrons. The actual result is obtained by subtracting the first probe current from the second one to subtract out the effect of the ion current, so that the spatial distribution of the high-energy electrons can be acquired. The results are shown in Fig. 11. The probe used in this measurement was similar to Probe 2; that is, its tip was shorter by 1 mm than that of Probe 2 to improve spatial resolution. The probe was maintained at -4 and 6 V with respect to cathode potential as the two sweeps were made. The contours are drawn every 100 μA. The number of the measuring points was 1656. Figure 11 shows that the high-energy electrons were concentrated near the centerline, and this fact coincides with the results shown in Figs. 9 and 10.

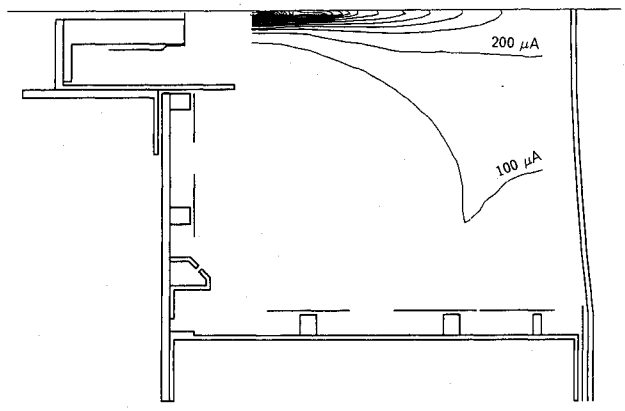

Fig. 11 Spatial distributions of high-energy electrons (Probe Current Contours).

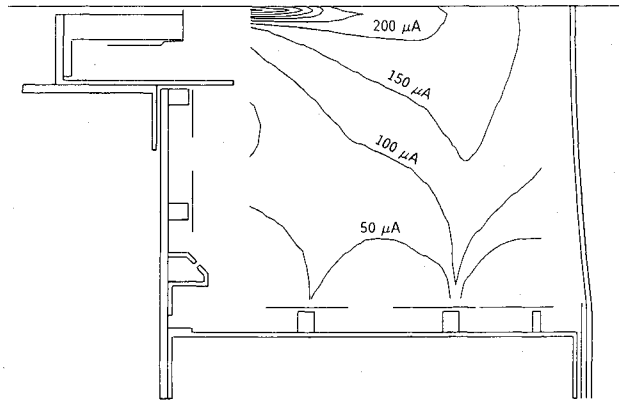

Fig. 12 Spatial distributions of ions (Probe Current Contours).

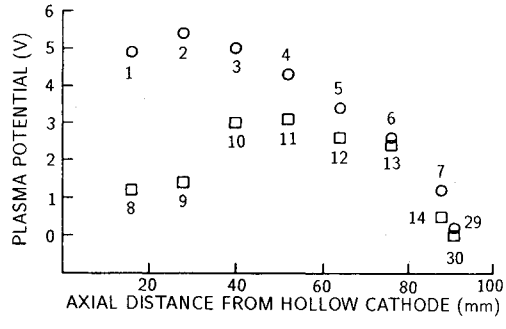

Fig. 13 Plasma potentials (axial variation).

Figure 11 also shows that the beam electrons flowed off the centerline of the discharge chamber or the probe did not trace the centerline.

The method just described represents an efficient and practical way to get the spatial distribution of the electrons whose energies are spread from the Maxwellian group. Getting the complete energy distribution at many points is, on the other hand, both difficult and impractical. Considering both the energy distribution data and the spatial distribution data gives a reasonable picture of the distribution of particles in the chamber.

Another advantage of this method is that the spatial distribution of ions is acquired at the same time. Figure 12 shows a contour map of the probe current in the case that probe is held at −4 V with respect to cathode potential and it should, therefore, correspond to ion concentration contours. The contours are drawn every 50 μA. Many ions are seen to concentrate near the centerline, where they appear to be produced in the electron beam.

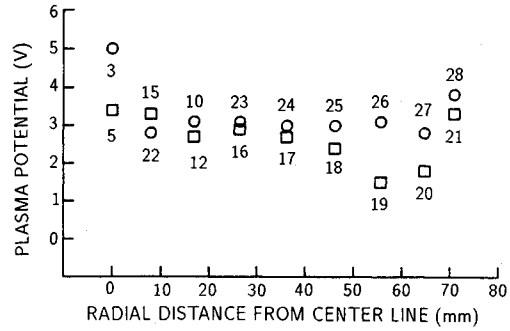

Fig. 14 Plasma potentials (radial variation).

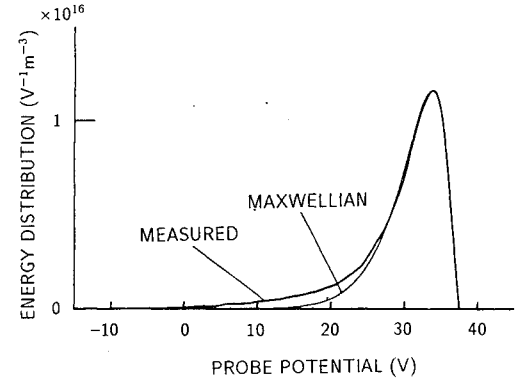

Fig. 15 Comparison of measured and Maxwellian distribution.

Plasma Potential

The axial and radial plasma potentials, measured with respect to anode potential, using Probe 1 are shown in Figs. 13 and 14. The plasma potential reaches a maximum value at PP 2 along the centerline. Ions produced downstream of there are forced toward the grids while ions produced upstream of there are forced toward the cathode. The situation along another line parallel to the centerline, from PP 8 through 15 and 30 is almost the same as that along the centerline. The plasma potentials are almost constant along the arcs through the weak field region (≤10 mT) except on the centerline where the electron beam produces many ions and, therefore, a higher plasma potential. Relatively high plasma potentials are shown at PP 21 and 28 where the probe is close to the wall of the discharge chamber. In these regions, electron densities are low because of the high magnetic field there, while ion densities are affected less and as a result the plasma potential is higher than it is in the bulk of the discharge chamber. This phenomenon facilitates ion confinement away from discharge chamber walls. Relatively low plasma potentials are shown at PP 19 and 20. The low-energy electrons flowing along the field lines toward the anode concentrate in this region, so that the potentials are lower.

Low Energy Electrons

Many of the electron energy distributions measured seem to include a Maxwellian electron component. Figure 15 shows the energy distribution measured at PP 18 and an ideal Maxwellian distribution having a peak that corresponds to the measured one. The measured distribution has more electrons than the Maxwellian one in high-energy region while they coincide in the lower energy region. This fact is common through all of the single-peak distributions. The electron energy distribution did not match an ideal Maxwellian distribution at any point in the discharge chamber.

Conclusion

Electron energy distributions were measured in the discharge chamber of an ion thruster. Primary electrons are emitted from the hollow cathode as a narrow beam and flow along the common centerline of both the discharge chamber and the hollow cathode. The primary electrons are not monoenergetic, that is, their energy distribution has some spread. A small portion of the electrons have a greater energy than they acquired while being accelerated away from the cathode. Probe shape does not have much influence on the measurement of low-energy electrons. Probe position with respect to the electron beam must be identified to discuss the primary electrons quantitatively. Ion density is high where primary electron density is high. Electron energy distributions do not become completely Maxwellian at any location in the discharge chamber.

Acknowledgment

The authors wish to acknowledge the help and advice of P. J. Wilbur and his students Verlin J. Friedly and Jeffrey M. Monheiser of Colorado State University.

References

[1]Hayakwa, Y., et al., "The Experimental Investigation on 12 cm Ring Cusp Ion Thruster," Proceeding of 15th International Symposium on Space Technology and Science, 1986, pp. 97–102.

[2]Martin, A. R., "Electron Energy Distribution in an Ion Engine Discharge," *Journal of Spacecraft and Rocket*, Vol. 8, No. 5, 1971, pp. 548–550.

[3]Shimizu, K., and H. Amemiya, "High Speed Measurement of the Energy Distribution Function by a Differentiator Using Delay Element," *Oyobutsuri*, Vol. 49, 1980, pp. 145–154 (in Japanese).

[4]Shimizu, K., and H. Amemiya, "Measurement of the Electron Energy Distribution Function in Plasmas Using a Delay Element Differentiator and a Digital Averager," *Oyobutsuri*, Vol. 51, 1981, pp. 971–978 (in Japanese).

[5]Amemiya, H., and Y. Sakamoto, "Diagnostics of Low Temperature Plasma by the Probe Method," *Shinku*, Vol. 28, 1985, pp. 177–192 (in Japanese).

[6]Kagen, Yu. M., et al., "Electron energy distribution in a contacted low-pressure arc. I. Probe measurements." *Soviet Physics Technical Physics*, Vol. 22, No. 3, 1977, pp. 345–349.

[7]Druyvesteyn, M., "Der Niedervoltbogen," *Zeitshrift für Physik*, Vol. 64, 1930, pp. 781–798.

[8]Kitamura, S., et al., "Vacuum Facility for Xenon Ion Thruster Testing," Proceedings of 16th International Symposium on Space Technology and Science, 1988, pp. 95–100.